Modeling individual variations in equiluminance settings

Jingyi He

Department of Psychology, Northeastern University, Boston, MA, USA ✉

Yesenia Taveras-Cruz

Department of Psychology, Northeastern University, Boston, MA, USA ✉

Rhea T. Eskew, Jr.

Department of Psychology, Northeastern University, Boston, MA, USA ✉

Recently, we reported measurements of heterochromatic flicker photometry (HFP) in 22 young observers, with stimuli that (nominally) modulated only L- and M-cones and were kept at (approximately) a constant multiple of detection threshold. These equiluminance settings were represented as the angle in the (L, M) cone contrast plane, with the *greenish* peak of the flicker in quadrant II and the *reddish* peak in quadrant IV; equiluminance settings were reported as the greenish angle. The mean equiluminance angle was 116.3° (an M:L cone contrast ratio of −2 at equiluminance), but individual differences in the settings were substantial, with the variation across individuals almost five times larger than the within-subject precision in the settings. In the present study we sought to determine the degree to which we could account for our observers' HFP settings by plausible variations in the macular pigment optical density (MPOD), the lens pigment optical density (LPOD), the cone photopigment optical densities (PPOD), and serine/alanine polymorphism in L-cone opsin (λ_{max} shift). Most of the range of our measured equiluminance angles could be accounted for by these factors, although the largest two angles (smallest $|\Delta M/M : \Delta L/L|$ ratio at equiluminance) could not. Individual differences in HFP have sometimes been taken to indicate variations in the ratio of L:M cone number; our results suggest that most of the individual differences in HFP might be equally well ascribed to physiological factors other than cone number. Simple linear models allow predictions of equiluminance angle, cone adapting level, and artifactual S-cone contrast from the values of the four factors considered here.

Introduction

The standard observer in color vision has long been used to characterize colorimetric properties of the human visual system and to make predictions about perceptual judgments. However, individual differences are generally too large for people to be represented by a single standard function, even among those who have intact visual systems. In color vision, models have been developed that include individual variations to better depict the actual performance of human color vision (Asano, Fairchild, & Blonde, 2016; Lee, Richardson, Walowit, Crognale, & Webster, 2020). Here, we focus on individual differences in equiluminance.

We aim to model the individual differences that we observed among the 22 observers in our recent work (He, Taveras-Cruz, & Eskew, 2020), in which we compared four methods of setting equiluminance: heterochromatic flicker photometry (HFP), minimum motion, and two variations on minimally distinct border settings. The stimuli were restricted to L- and M-cone modulations, based upon the Stockman-Sharpe cone fundamentals (Stockman & Sharpe, 2000), and were kept at approximately constant multiples of detection threshold. Cone contrasts were used to account for the effects of cone-specific adaptation. These normal trichromatic observers used the method of adjustment to set the angle (the ratio of M:L cone contrasts) minimizing the sensation of flicker (HFP), motion, or border distinctness. These equiluminance settings were represented as the angle in the LM cone contrast plane, with the *greenish* peak of the flicker in quadrant II and the *reddish* peak in quadrant IV; equiluminance settings were reported as the greenish angle (Figure 1a). In the present study we focus on the method that we found to be most precise and reliable, heterochromatic flicker photometry (HFP). In the HFP experiment, the grey background was set to 75 cd/m^2 at chromaticity coordinates (0.289, 0.315), and produced an M_{adapt}/L_{adapt} ratio of 0.86. The test field was a 2° × 2° square patch, sinusoidally flickering around gray (75 cd/m^2) at 10.63 Hz. Observers set the equiluminance angle at two different contrast levels, a total of 20 HFP settings per observer divided over two sessions (four observers only completed one of the sessions).
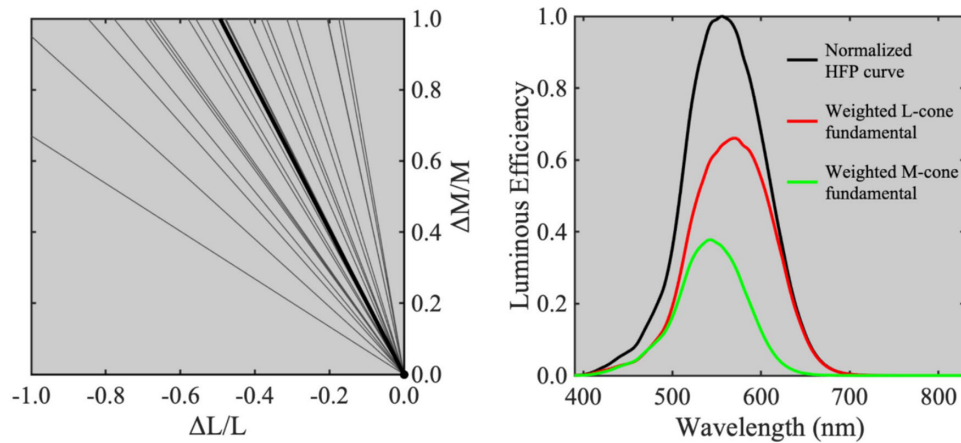
Figure 1. Angle in the cone contrast space transformed to the corresponding V(λ) function. (a) Left panel: the 22 thin black lines represent the HFP setting of the observers in He et al. (2020) presented in the second quadrant of the LM cone contrast plane, and the thick black line is the average of these settings. The horizontal and vertical axes are L-cone contrast and M-cone contrast, respectively. The origin of the plane is at the bottom right corner. (b) Right panel: the black curve represents the normalized V(λ) function transformed from the mean angle in (a), the two components of which are indicated by red (weighted L-cone fundamental) and green (weighted M-cone fundamental) curves. See He et al. (2020) for details.

Data from these 22 observers have some advantages for the purpose of modeling. First, the stimuli were all kept at nearly constant multiples of detection threshold, minimizing any irrelevant changes in perceived stimulus strength. Second, the adapting state of the observers was unlikely to have been altered by variations in the test stimuli, unlike the customary HFP experiment with monochromatic lights (see Sharpe, Stockman, Jagla, & Jägle, 2011 and He et al., 2020 for discussion). Third, the stimuli were constructed to modulate the L- and M-cones of a standard (Stockman-Sharpe) observer, so that variation in the results is easily represented as deviations from that standard observer.

In our data, the mean equiluminance angle from HFP is $\alpha_{HFP} = 116.3°$[1] (Figure 1a). This equiluminance angle can be transformed to a luminosity function as the black curve in Figure 1b (see detailed discussion in He et al., 2020), which was obtained by summing the weighted L- and M-cone fundamentals. Consistent with prior results (e.g., Gibson & Tyndall, 1923; Sharpe, Stockman, Jagla, & Jägle, 2005; Sharpe et al., 2011), our observers showed substantial individual differences in their HFP settings, with observers having α_{HFP} ranging between 99.3° and 146.2°, corresponding to M:L cone contrast ratios of −6.1 and −0.7. The variation across individuals was almost five times larger than the average within-subject precision in the settings.

Physiological and anatomical sources of variability contribute to individual differences in equiluminance measured by HFP. The filtering effect of the ocular media, primarily the lens, and the effect of the macular pigment, play a major role in altering equiluminance settings (Lee et al., 2020). Other pertinent differences between observers are shifts in the peak absorbance of the cones due to gene polymorphisms, the most common shift being due to a serine/alanine substitution at position 180 in the L-cone gene (Merbs & Nathans, 1992; Sharpe, Stockman, Jägle, Knau, Klausen, Reitner, & Nathans, 1998), and variations in the relative peak density of L-, M-, and S-cone photopigment. These four factors—macular pigment optical density (MPOD), lens optical density (LPOD), photopigment optical density (PPOD), and L-cone peak absorbance shifts (L-λ_{max} shift)—are the focus of the present work. We aim to understand how these factors may have contributed to the individual differences observed in our study, specifically, and for other observers and stimuli more generally. To do this, we begin by making a provisional assumption—that all observers are identical postreceptorally (with regard to their HFP settings) and differ only in their cone fundamentals (due to plausible variations in MPOD, LPOD, PPOD, and L-λ_{max} shift). We name this the "neural equiluminance constancy" assumption. This assumption means that if we model the response of the luminance mechanism for *observer i* as a weighted sum of cone contrasts

$$Luminance\ Response = k_1\left(\frac{\Delta L}{L}\right)_i + k_2\left(\frac{\Delta M}{M}\right)_i, \quad (1)$$

the relative weighting of the L- and M-cone responses k_1/k_2 is the same for every observer, such that at equiluminance (zero luminance response)

$$\left(\frac{\Delta M}{M}\right)_i = -\frac{k_1}{k_2}\left(\frac{\Delta L}{L}\right)_i \quad (2)$$

The slope of this line is the cone contrast ratio at equiluminance. The subscript i is used to indicate that the cone contrasts are based upon the observer's own cone fundamentals. The equiluminance angle in the second quadrant of observer's own ($\Delta L/L$, $\Delta M/M$) plane is

$$\alpha_{HFP} = 180° + tan^{-1}\left(-\frac{k_1}{k_2}\right) \quad (3)$$

and is therefore the same for every observer (in their individual cone contrast plane).

We use cone contrasts here to represent stimuli. The Appendix describes how our analysis would be applied to cone excitations (in either arbitrary or threshold units) rather than cone contrasts. Our conclusions would be the same had we used cone excitation rather than contrast, assuming the observer's chromatic adaptation was kept constant (Eskew, McLellan, & Giulianini, 1999; see He et al., 2020 for discussion).

Changes in the relative contributions of L- and M-cones to the luminance response (the k_1/k_2 ratio) might reflect neural factors in the retina, lateral geniculate nucleus, or cortex, but a common interpretation of variations in HFP settings is an anatomical one: that individual differences in HFP are due to differences in the numbers of L- and M-cones (e.g., Brainard et al., 2000; Gunther & Dobkins, 2002; Kremers et al., 2000; Rushton & Baker, 1964). Our primary goal is to study how much of the variation across individuals can be accounted for by the neural equiluminance constancy assumption alone. This assumption may be interpreted as a purely computational convenience: it allows us to calculate the changes in equiluminance that can be achieved *without* changes to k_1/k_2 (*any* equiluminance angle can be achieved by changing the k_1/k_2 ratio); compare Bieber, Kraft, and Werner (1998), who fixed the L/M ratio for similar reasons. We are agnostic as to whether there might be changes in k_1/k_2 in addition to changes in cone fundamentals, and also as to whether, if there are changes to k_1/k_2, they would reflect variation in cone number or in other neural factors. The implications of our modeling for understanding effects of relative cone number, and of possible interpretations of neural equiluminance constancy, are briefly discussed in the Conclusions section.

Chromatic transforms and the neural equiluminance constancy assumption

Under the neural equiluminance constancy assumption, the observed variation we obtained in

equiluminance angle (He et al., 2020) is attributed solely to the fact that we used the Stockman-Sharpe cone contrast space for observers whose cone fundamentals were not the Stockman-Sharpe ones, both to construct the stimuli and to analyze the data. As in our prior work, we represent the results in the second quadrant of the LM plane (there is an equivalent result 180° away, at the other peak of the flicker, in Quadrant IV). The mean α_{HFP} for our 22 observers is 116.3° (standard deviation = 12.4°). Using that mean angle in Equation 3 implies a relative cone contrast weighting of $k_1/k_2 = 2.03 \approx 2$, such that L-cones contribute twice as much as M-cones to the response underlying HFP. Specifying a particular k_1/k_2, along with the neural equiluminance constancy assumption, permits us to quantitatively estimate the contributions of the individual difference factors that determine the shapes of the cone fundamentals.

Figure 2 illustrates our modeling process. The second column shows three example model observers' cone fundamentals, with the middle panel being the Stockman-Sharpe (Stockman & Sharpe, 2000; Stockman, Sharpe, & Fach, 1999) fundamentals. Red, green, and blue curves represent L-, M-, and S-cone fundamentals. The top and bottom large panels show cone fundamentals for two other model observers that represent extreme combinations of the four individual difference factors. The small panels show the differences between those model observers and the Stockman-Sharpe standard observer. For illustration here, observer O_A and observer O_Z represent the maximum and minimum values of MPOD, LPOD, PPOD, and L-λ_{max} shift, producing extreme equiluminance angles in different directions. The values of their *prereceptoral factors* are represented as PRF_A and PRF_Z in the first column, respectively. Similarly, the prereceptoral factors for the standard observer O_{SS} are represented by PRF_{SS}.

The panels within the dashed box in Figure 2 describe the steps from individual cone contrasts to results analyzed in standard cone contrasts. Colors used in the dashed box are chosen arbitrarily and do not refer to cones or stimuli. The middle row shows, in yellow, the plane of zero S-cone contrast for the standard observer, and the corresponding plane in the RGB primary space of our display (see Appendix). The three yellow planes in the middle row represent the same set of stimuli. In our experiment, stimuli were restricted to this plane (He et al., 2020): the stimuli were designed to leave the S-cones of the standard observer unmodulated. The three points in RGB space represent, schematically, three HFP settings (at one flicker peak) for Observers A, SS, and Z, all lying on the outer edges of the yellow plane.

The first column within the dashed box represents the L-, M-, and S-cone contrasts for each of the three observers at equiluminance in their *individual cone contrasts* (S-cone contrast is zero for Observer
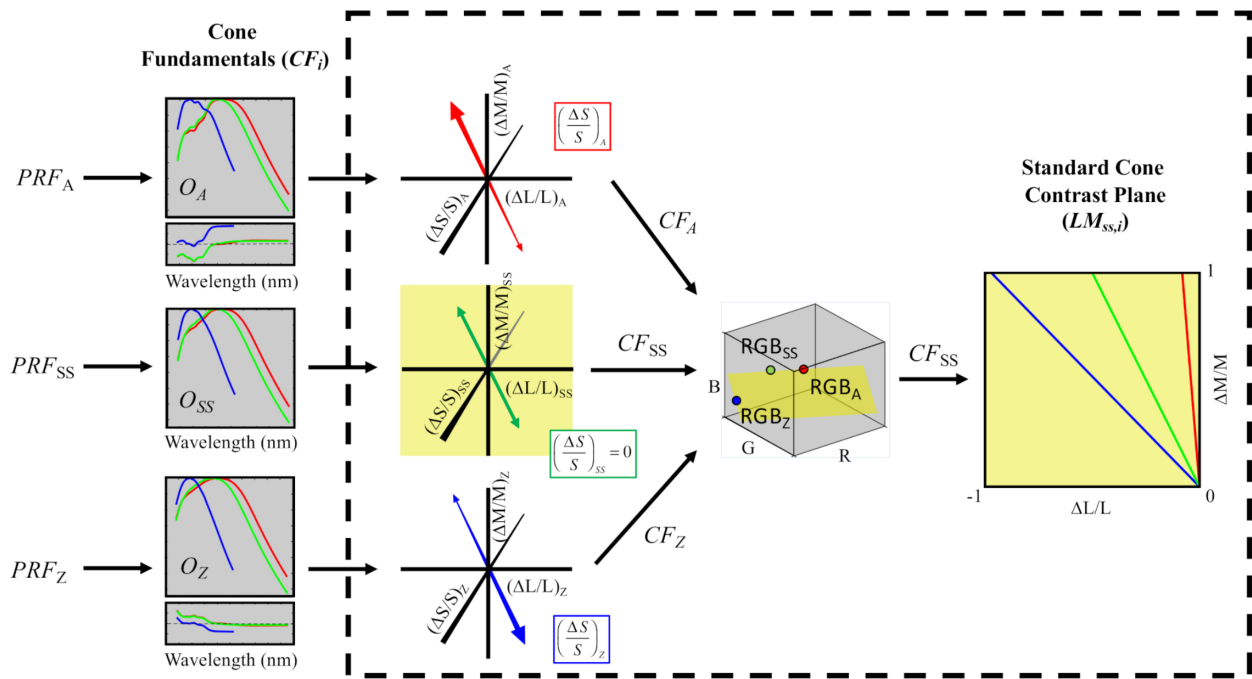
Figure 2. Modeling process. The main procedures representing transmission from individual cone contrasts to standard cone contrasts are given within the dashed box. Each row represents an observer (A, SS, and Z), with SS being the standard. Columns from left to right each represent prereceptoral factors (PRF), cone fundamentals (CF), individual LMS cone contrast spaces, primary (RGB) settings, and measured results represented in the second quadrant of the standard LM cone contrast space (origin at bottom right of the box). All model observers have M:L cone contrast ratios of -2 at equiluminance (slope of colored arrow projected into the zero S-cone contrast plane) in their individual cone contrast space. The yellow plane in the standard observer's cone contrast space has zero S-cone contrast; the corresponding plane in RGB primary space is also shown in yellow. The HFP experiment used stimuli lying in this RGB plane. The red, green, and blue colors in the dashed box indicate the three observers; the colors do not refer to cones or stimuli. See text for details.

SS). The cone contrasts produced by the flicker at the HFP settings are indicated by the double-headed colored arrows; these all have $-2:1$ M:L in their individual cone contrasts (an application of the neural equiluminance constancy assumption). The RGB settings corresponding to that 2:1 ratio are shown as three dots in RGB space, in the yellow plane representing all the stimuli used in the experiment. The green arrow lies in the plane of the page because experimental stimuli produce zero S-cone contrast for the standard observer. This is not necessarily the case for nonstandard observers. Red and blue arrows are tilted out of the plane of the page to suggest the production of S-cone contrast by the RGB settings of the nonstandard observers. The double-headed arrows and dots are drawn to attempt to clearly illustrate the ideas and are not intended to accurately represent the cone contrasts or RGB settings (a more accurate rendition of the RGB plane is given in Figure A2).

The computation finds the unique RGB triplet, for a given model observer, that lies at the edge of the yellow plane and produces a $-2:1$ M:L contrast ratio in terms of the observer's individual cone fundamentals. These RGB$_i$ are transformed to the standard LM

cone contrast plane using the Stockman-Sharpe fundamentals, as done by He et al. (2020) in analyzing experimental results. The three example equiluminance angles are indicated by the red, green, and blue lines in quadrant II of the standard cone contrast LM plane at the far right. These $LM_{SS,i}$ cone contrast angles are what we reported as equiluminance settings (He et al., 2020); in the current study we examine the influence of the preretinal factors on these settings. In addition, we analyze the unwanted S-cone contrasts produced for these observers by stimuli that were designed to have zero S-cone contrast for the *standard* observer.

The formal treatment of the model, described in the Appendix, finds the intersection of two planes in the RGB primary space. One plane comprises all the RGBs that produce $(\Delta M/M)_i/(\Delta L/L)_i = -2$ for a given observer. The other plane in RGB is defined by $(\Delta S/S)_{SS} = 0$ for the standard observer, illustrated in yellow in Figure 2. The intersection of those two planes is a line; the RGBs along that line satisfy the neural equiluminance assumption for that observer as tested with the experimental stimuli.

Therefore, our research question is to ask whether plausible variations in cone fundamentals alone are

Source of variation	Minimum	Standard	Maximum
MPOD	0	0.35 (at 460 nm)	1.2
LPOD	0.75×1.765	1.765 (at 400 nm)	1.25×1.765
PPOD $_{[L,M,S]}$	[0.4, 0.4, 0.32]	[0.5, 0.5, 0.4]	[0.8, 0.8, 0.64]
L-cone λ_{max}	$545 - 1.5$ nm (left-shifted)	545 nm	$545 + 1.5$ nm (right-shifted)

Table 1. The variation ranges selected for the four physiological factors. The standard value and the two ends of the ranges are listed here.

sufficient to account for the variations in equiluminance across our real observers. Computations were performed using the measured emission spectra of the monitor from our previous study, a SONY GDM-F520 CRT monitor (Tokyo, Japan). Those primaries are depicted in Figure A1 of the Appendix.

In addition to computing the equiluminance angles and S-cone contrasts, we also compute the changes to cone adapting levels resulting from changes in cone fundamentals. These adapting levels are the denominators in the cone contrasts and represent (in arbitrary units) the quantal catches produced by the gray, mean field condition (background and mean of the flicker) in our experiment. For example, increases in cone photopigment optical density will not only change the shape of the fundamental, but also increase the average level of quantal catch experienced by the photoreceptor. Of course, this change in cone adapting level has no effect upon the cone contrasts, since both numerator and denominator of the cone contrasts are calculated with the altered fundamental, so the changes in adapting level are reported separately.

The results of our modeling indicate that almost all of the variation in our equiluminance settings can be accounted for by variations in cone fundamentals alone (the neural equiluminance constancy assumption). Moreover, although our stimuli were designed to leave the S-cones unmodulated for a Stockman-Sharpe observer, artifactual S-cone modulations would be created for nonstandard observers. We provide simple linear descriptive models to relate equiluminance angle, S-cone contrast, and cone adaptation level, to values of the four individual difference factors.

Selection of variation ranges for physiological factors

The following paragraphs explain how the variation ranges for physiological factors were selected. These ranges are summarized in Table 1. In selecting these values, we emphasized results based upon the central 2° of the retina.
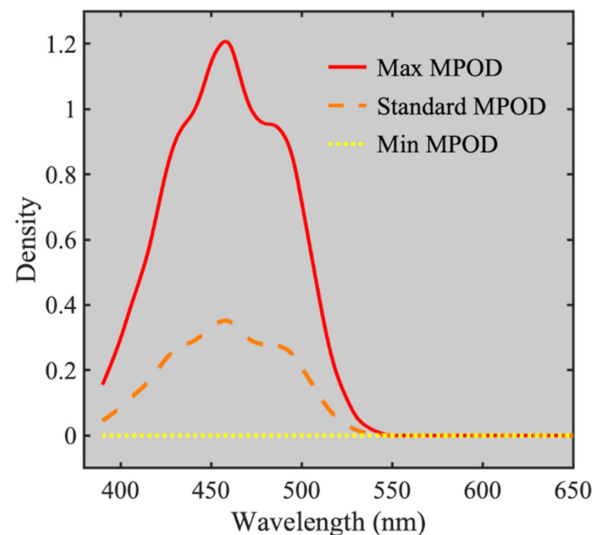

Figure 3. The standard MPOD curve, based upon Bone, Landrum, and Cains (1992), is shown in a dashed orange curve, which has a peak density of 0.35 at 460 nm. The solid red and dotted yellow functions represent the upper (peak = 1.2) and lower (peak = 0) bounds of the MPOD range used.

Macular pigment optical density (MPOD) is one of the most influential factors affecting spectral sensitivity (Stockman & Sharpe, 2000; Stockman et al., 1999). It is also a key factor for maintaining a healthy retina. For example, age-related macular degeneration is correlated with low macular pigment density (Beatty et al., 2001). The standard MPOD curve we adopted is the one developed by Stockman et al. (1999) which has a peak density of 0.35 at 460 nm for a 2° observer. As reviewed in Stockman et al. (1999), macular density can vary within a large range of 0 to 1.2 at 460 nm (Bone & Sparrock, 1971; Pease, Adams, & Nuccio, 1987). Therefore, the two extreme values we selected were 0 and 1.2 for density at 460 nm (Figure 3).

Lens pigment optical density (LPOD) is also a critical factor determining cone spectral sensitivity (Stockman & Sharpe, 2000; Stockman et al., 1999). This density varies substantially with age (Pokorny, Smith, & Lutze, 1987). Given that the ages of our observers were all between 18 and 30, variation in lens optical density was
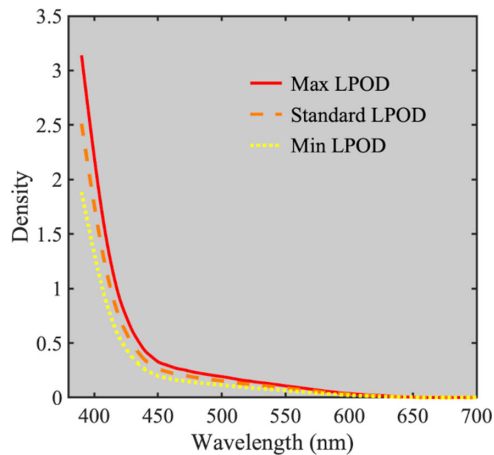
Figure 4. The standard LPOD curve is shown in a dashed orange curve which has a density of 1.7649 at 400 nm. The solid red and dotted yellow curves represent the upper and lower bounds of the LPOD range selected, which are 25% higher and lower than the standard, respectively.
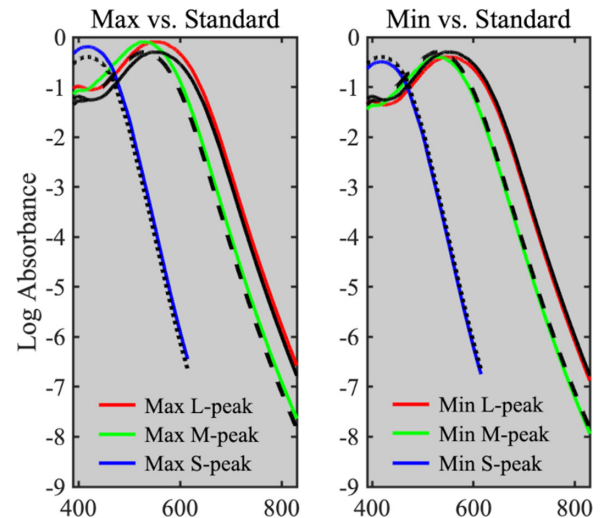

Figure 5. In both panels, the standard L-, M-, and S-cone photopigment optical density spectra are plotted as solid, dashed, and dotted black curves, and the rescaled density spectra for L-, M-, and S-cones are plotted in solid red, green, and blue, respectively. The panels show the upper (left panel) and lower (right panel) bounds of PPOD curve variation. The peaks are not normalized to illustrate how density affects the heights as well as the shapes of the curves.

not considered likely to be a major factor in explaining our equiluminance ranges, but we have included it for generality. The standard LPOD curve was adopted from Stockman et al. (1999) which has a density of 1.7649 at 400 nm (Figure 4). Since the density was reported to vary approximately ±25% around the average in young observers, we adopted this variation range around the standard density at 400 nm (Norren & Vos, 1974).

Photopigment optical density (PPOD) can be estimated by several different methods, providing different but overlapping estimates for the PPOD (see cvrl.org for a summary table). The critical factor that affects PPOD, the length of the outer segment of the cone photoreceptors, varies with eccentricity, and outer segments of S-cones may be shorter compared to L- and M-cones (Sharpe et al., 1998). Stockman and Sharpe assumed that for their mean 2° observer, L-, M-, and S-cone density peak was 0.5, 0.5, and 0.4, respectively (Stockman & Sharpe, 2000). Therefore, we used these values as the standard peak density for each cone type, and 0.4 and 0.8 were selected as the lower and upper bounds of L- and M-cone density (based upon Berendschot, van de Kraats, & van Norren, 1996); the corresponding S-cone density was always 20% lower (see Figure 5).

Our focus is primarily on how variation in the four factors alter the shapes of the cone fundamentals and thus change the modulations of the cones in response to the primary lights, which is why we use cone contrasts. However, there are also effects of the four factors on the *mean* or adapting level of cone responses, and these effects are not captured by contrasts. High values of both MPOD and LPOD will lower the average

light level reaching the cones and thus reduce their adaptation level. On the other hand, increases in PPOD will, by increasing quantal catch, tend to have the opposite effect. We calculate the adaptation state for each cone type for all the model observers. To the degree that cone-independent (von Kries) adaptation applies to our conditions (likely a high degree, given the constant gray background of approximately 2.6 log Td), these changes in adaptation are not very important, but we report them for completeness in the Results section (see *Adaptation state* section and Figure 11, and Equation A3).

Lastly, a change in the wavelength of peak absorbance of a photoreceptor (λ_{max}) may be produced by cone opsin gene polymorphisms. The most common polymorphism is the substitution of alanine for serine at position 180 in the L-cone photopigment gene, which leads to a shift of approximately 3 nm for normal subjects (Neitz & Jacobs, 1990; Sharpe et al., 1998). The Stockman-Sharpe fundamentals, used as our standard, are based upon pooling observers with both the ala180 and ser180 polymorphisms. Therefore, the range we adopted for λ_{max} shift of the L-cone fundamental was minus 1.5 nm (left-shifted) to plus 1.5 nm (right-shifted), such that the midpoint (no shift) corresponds to the Stockman-Sharpe L-cone average (545 nm). The differences between the extreme cases and the standard curve are shown in Figure 6. Less common polymorphisms are not considered here.
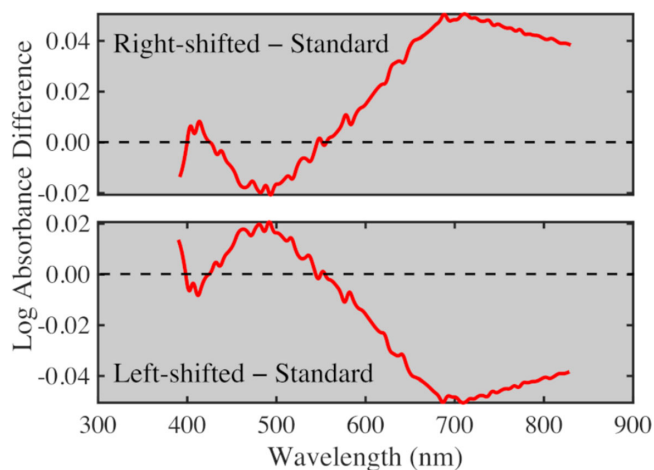
Figure 6. The red curves in the upper and lower panels show differences between the standard L-cone absorbance curve and the right-shifted (top panel) and left-shifted (bottom panel) L-cone absorbance curve.

Results and discussion

α_{HFP} range accounted for by each factor

We first calculated the α_{HFP} range that each factor alone can account for. With MPOD, LPOD, PPOD, and L-λ_{max} shift in turn being the only source of variability, the ranges they can explain are 14.75°, 7.25°, 16.00°, and 7.25°, respectively. The top row of Figure 7 shows nine example α_{HFP} produced by values of each factor within the selected range. The green cross represents the α_{HFP} calculated from the standard value of the factor, and the blue and red dots represent the upper and lower bounds of the α_{HFP} range. The other colored dots represent other intermediate α_{HFP}. As the value chosen for the factor (density or λ_{max}) increases, α_{HFP} decreases for all factors. The change is nearly linear, with PPOD and MPOD having the steepest decreasing slopes. The bottom row of Figure 7 represents these ranges in the LM plane of the standard Stockman-Sharpe cone contrast space. In each panel, the standard observer is represented by the green central line. The red line represents the lower bound of the range the factor can explain, which has a smaller angle compared to the standard; whereas the blue line represents the upper bound, which corresponds to a larger angle. The angles falling within the range covered by the red and the blue lines represent the HFP settings this factor can account for. Figure 8 plots these ranges as bars, with the standard angle ($\alpha_{HFP} = 116.3°$) being represented as green dots. The two vertical axes indicate the angle in QII and the M:L cone contrast ratio at each tick mark. Changes in MPOD and PPOD account for larger changes in α_{HFP} while LPOD and L-λ_{max} shift produce

relatively small changes. Note that only the two extreme values of L-λ_{max} shift refer directly to the serine/alanine polymorphism; the intermediate values are calculated for completeness.

Cone fundamentals are, of course, special cases of color matching functions. Color matching functions have been shown to share the same sources of variation with the luminosity function (Lee et al., 2020; but see Rushton & Baker, 1964, discussed in the Conclusions section). It has been suggested that the primary sources of individual variability in color matching functions are likely to be density variations in the macular pigment and the lens (Asano et al., 2016; Golz & MacLeod, 2003; Lee et al., 2020; Webster & MacLeod, 1988). Since our observers were young, we varied LPOD only by 25% and the effect was correspondingly small, but we do see a large change due to MPOD. In our model, PPOD produces the largest changes in α_{HFP}.

As shown in Figures 7 and 8 (right axis), high values of MPOD, LPOD, and PPOD, and increases in L-cone λ_{max} mimic the effects of increases in relative L-cone input (the M:L cone contrast ratio) into a luminance mechanism. The density increases reduce the observer's sensitivity to the blue and green primary lights relative to the red light; the increases (right shift) in L-cone λ_{max} promotes the sensitivity to the red light. Both increases therefore cause the model observer to move in a deuteranopic direction (a deuteranope would set α_{HFP} at 90°). Decreases in the values of the four factors from the standard have the opposite effects, moving the α_{HFP} in a protanopic direction.

α_{HFP} range accounted for by all factors

The colored lines in Figure 9 show the results when all the factors are allowed to vary simultaneously. The four factors cause the equiluminance angle to vary from 91.5° to 134.0° (a range of 42.5°); no combination of the four factors would produce angles outside of this band (using our selected ranges of values). These angles cover almost all of the range of the actual observers' settings (thin lines in Figure 9). The angles of our two most extreme observers (136.5° and 146.2°), with high M:L contrast at equiluminance (cone contrast ratios of -0.95 and -0.67), are larger than the largest angle produced by our model. However, M:L ratios this extreme, measured using different methods from ours, are not uncommon among the normal population (Carroll, Neitz, & Neitz, 2002; Sharpe et al., 2005).

The failure to account for the settings of two observers ($\sim$10% of our data; Figure 9) could have several causes. First, the settings made by these two observers have standard deviations larger than most of our observers. Therefore, these extreme angles may represent measurement error. Second, it is possible these two observers had other cone polymorphisms
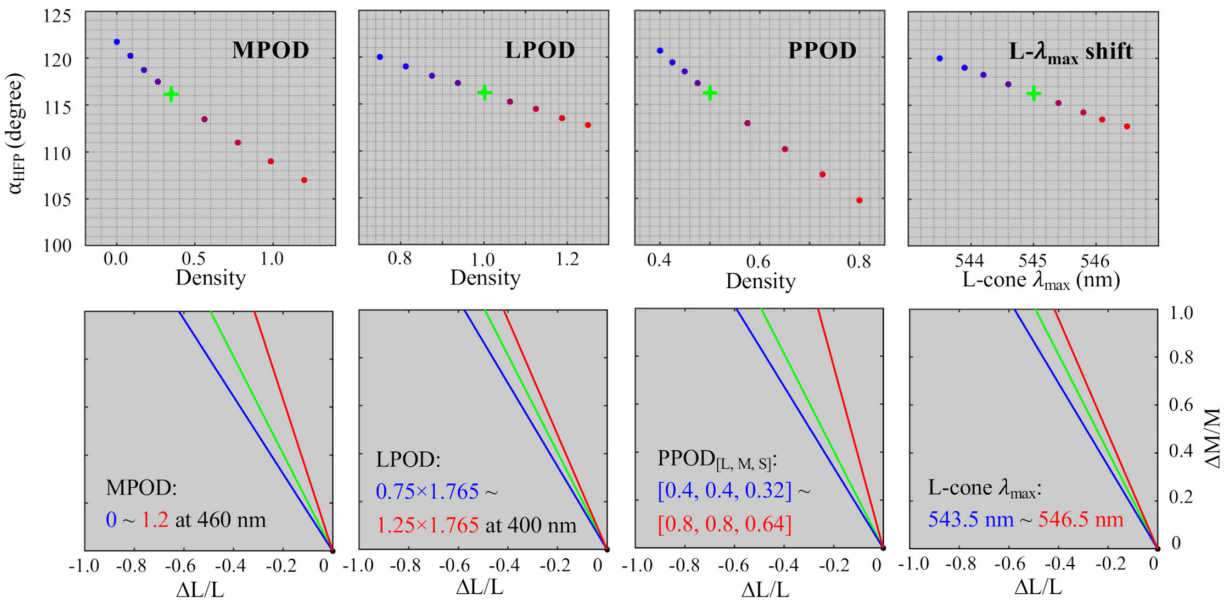
Figure 7. Ranges in α_{HFP} that each factor can account for when considered individually. Each panel in the top row shows nine examples of α_{HFP} spanning the selected ranges of the factor (note differences in horizontal scale). The blue dot and red dot at the two ends in each panel are the maximum and minimum α_{HFP}, and the green cross represents the α_{HFP} produced by the standard value (the mean of the real settings). The other dots are intermediate α_{HFP}. The horizontal axis for the PPOD panel represents photopigment density of L- and M-cones; S-cone density was always 20% lower. The bottom row represents extreme and standard α_{HFP} in the 2nd quadrant of the LM plane. The horizontal axis and the vertical axis in each panel are $\Delta L/L$ and $\Delta M/M$, with the origin at the lower right of each panel. The central, green line represents the standard observer, and the blue and red lines represent the upper and lower bound of each α_{HFP} range. The ranges labeled in the panels indicate the selected ranges of the factors that produce the corresponding α_{HFP}.
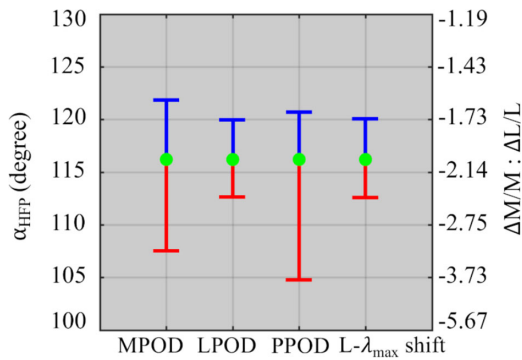

Figure 8. Ranges in α_{HFP} that each factor can account for individually. The green dots represent the standard observer. The vertical axis on the left indicates α_{HFP} in the LM plane (quadrant II) and the vertical axis on the right indicates the corresponding M:L cone contrast setting at equiluminance, which is equal to the negative of the k_1/k_2 ratio (Equation 2). The cone contrast ratio axis is not a linear scale.

than the serine/alanine one in L-cones that we have considered. Third, these observers might have unusually low lens density or photopigment optical density (see next paragraph). Fourth, this could represent a failure of the neural equiluminance constancy assumption, suggesting that the k_1/k_2 ratio has to be altered
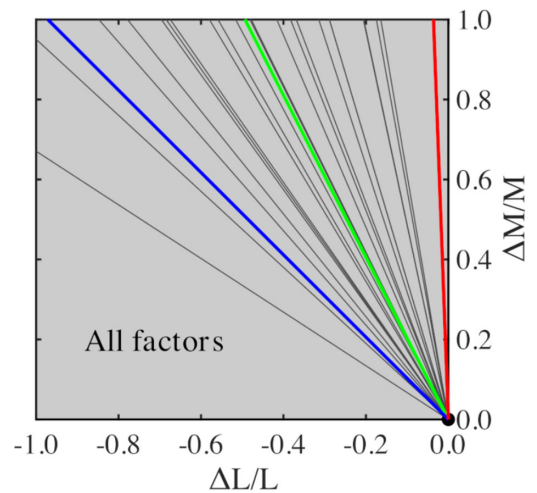

Figure 9. Range in HFP settings accounted for when all factors are considered together. The black lines indicate the settings made by the 22 real observers in (He et al., 2020). The central green line represents the standard observer (and the mean of the real settings), and the red and blue lines represent the two extreme model observers. These equiluminance settings fall between 90° (equivalent to a deuteranopic setting) and 180° (equivalent to a protanopic setting); the red line (maximum values for the four factors) approaches the deuteranopic setting.

| Factors | | | | | |
MPOD	LPOD	PPOD $_{[L,M,S]}$	L-λ_{max} shift (nm)	Angle	M:L ratio
<u>0</u>	1.765	[0.5, 0.5, 0.4]	0	121.75°	−1.616
0.35	<u>0</u>	[0.5, 0.5, 0.4]	0	131.25°	−1.140
0.35	1.765	<u>[0.01, 0.01, 0.008]</u>	0	139.75°	−0.847
0.35	1.765	[0.5, 0.5, 0.4]	<u>−1.5</u>	120.00°	−1.732
<u>0</u>	<u>0</u>	[0.01, 0.01, 0.008]	<u>−1.5</u>	159.25°	−0.379

Table 2. The largest equiluminance angles (lowest absolute M:L cone contrast ratio) that can be produced by varying only one factor and all factors. Each of rows 1–4 has one factor set to the lowest possible value (underlined) and other factors fixed at standard. All factors are set to the minimum in the bottom row.

(Equation 3). Of course, variations in the k_1/k_2 ratio can produce any equiluminance angle, including the two most extreme that we observed. To produce the largest angle we observed (146.2°), while keeping the four factors at the minimum values of the ranges specified in Table 1, requires changing the k_1/k_2 ratio from 2.0 to 1.185.

Angles further in the protanopic direction than the largest produced by our selected range of factors, 134.0°, can be produced by even lower LPOD or PPOD values. Our model includes a macular pigment density of zero, so the observers could not have a lower value of that factor (Table 1). The L-cone λ_{max} shift in our model is restricted to the serine/alanine L-cone polymorphism at position 180, so a left shift of 1.5 nm produces the largest possible equiluminance angle. However, if an observer had zero lens density (an extreme and hypothetical situation), the equiluminance angle would be 144.75° with other factors fixed at the lowest of the selected ranges. An implausibly low PPOD can produce angles as low as 151.25° in combination with the extreme values for the other factors shown in Figure 7. The lowest LPOD and PPOD, with the other two factors fixed at the lowest of the selected ranges, result in an equiluminance angle of 159.25° (Table 2, bottom row). This angle is the largest equiluminance angle (lowest absolute M:L cone contrast ratio) that can be produced after assuming a fixed k_1/k_2 of 2. Thus, our model can produce the entire range of angles observed in He et al. (2020) by use of extreme, and perhaps implausible, values of LPOD and PPOD.

A linear model

The modeling process outlined in Figure 2 requires extensive computation to produce new cone fundamentals and calculate the effect of the monitor primary lights on these fundamentals. Therefore, we also asked if a purely functional model can be derived to describe the relationship between the four variables and the equiluminance angle, without having to generate cone fundamentals at all (i.e., skipping the steps in columns 2–4 in Figure 2). The remarkable near linearity shown in the top row of Figure 7 suggests a linear model. To derive a model, we first generated 6561 model observers, each with a unique combination of the four factors within our selected ranges (nine levels of each) and therefore a unique set of cone fundamentals. These model observers (6560 of which are nonstandard observers) were used in the calculations outlined in Figure 2. Using this large set of computations, we found that we can describe the relationship between α_{HFP} and the values of MPOD, PPOD, LPOD, and L-λ_{max} shift (−1.5 to +1.5 nm) as

$$\alpha_{HFP} = 154.79 - 11.95\,MPOD - 7.94\,LPOD$$
$$- 39.38\ PPOD - 2.32\ \text{L-}\lambda_{max}\ \text{shift} \qquad (4)$$

(producing an $R^2 = 0.99$). The linear model can account for angles from 87.95° to 132.01° using the chosen ranges of the variables, without computing cone fundamentals at all. The values of the coefficients depend on our assumed $k_1/k_2 = 2$ ratio and our monitor primaries, but the general form is likely to be generalizable to other k_1/k_2 ratios and primary stimuli. The degree of linearity between the combination of these four factors and the equiluminance angle is remarkable and surprising.

S-cone modulation

Our experiment used stimuli that were designed to not produce any S-cone modulation for a Stockman-Sharpe observer, using the silent substitution method (Estévez & Spekreijse, 1982). The plane in RGB space in which L- and M-cones are modulated but S-cones are not depends upon the observer's L- and M-cone fundamentals (Appendix, Equation A8). Thus, the S-cones of observers who do not have the standard L- and M- cone fundamentals would have been modulated in our study. We calculated how much S-cone modulation was produced in our 6561 model observers at equiluminance (see details in Appendix).
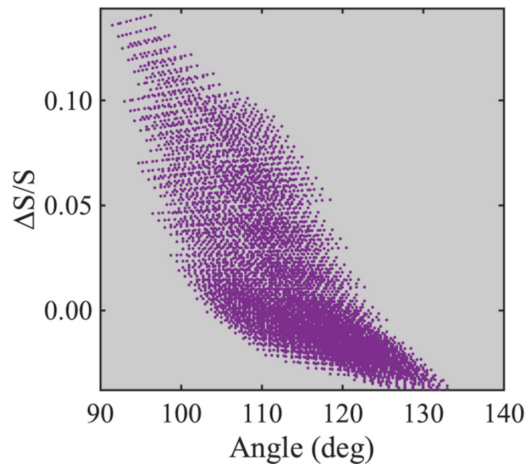
Figure 10. S-cone contrasts for the 6561 model observers. Each dot represents a model observer. The horizontal axis is the equiluminance angle in the standard LM plane and the vertical axis represents the S-cone modulation produced in a given model observer. See text for explanation of the sign of the S-cone contrast.

Figure 10 shows S-cone contrast produced for the model observers, using their own cone fundamentals (Figure 2). The sign of the S-cone contrast indicates the phase of the S-cone flicker produced by the flickering HFP stimuli: positive S-cone contrasts mean the S-cone flicker is in-phase with the M-cone flicker, negative contrasts mean the two are in antiphase (the phase relationship is reversed with the L-cones, since M-cones and L-cones are in antiphase for stimuli in Quadrants II and IV of the LM cone contrast plane). Model observers with small equiluminance angles (especially angles $< 100°$) produce larger S-cone contrasts. This means that the largest positive S-cone contrasts are associated with the largest MPOD, PPOD, and LPOD values we modeled; smaller than standard values of these preretinal factors do not produce negative S-cone modulations of corresponding magnitudes.

The same set of 6561 model observers was used to model the effects of the four factors on S-cone contrast, and a similar linear model works remarkably well:

$$\frac{\Delta S}{S} = -0.115 + 0.089 \ MPOD + 0.029 LPOD$$
$$+ 0.065 \ PPOD \qquad (5)$$

($R^2 = 0.98$). Note that L-λ_{max} shift makes no contribution.

Under neutral adaptation conditions such as used in our experiment, S-cones do not contribute to heterochromatic flicker photometry (Ripamonti, Woo, Crowther, & Stockman, 2009), and S-cone sensitivity is low at the 10.63 Hz temporal frequency used (Stockman, Langendörfer, & Sharpe, 2007; Stockman, MacLeod, & DePriest, 1991). Therefore, it is unlikely

that the S-cones would have made direct contributions to the HFP settings made by our real observers. But at lower temporal frequencies many of these S-cone contrasts would clearly be above threshold.

The results in Figure 10 and Equation 5 could be used to exclude observers from a study when artifactual S-cone stimulation is a concern. For an example, an observer who sets an equiluminance angle between approximately 105° and 125°, or has an M:L contrast ratio at equiluminance between -3.7 and -1.4, produces an artifactual S-cone contrast of less than about ± 0.01 with a display like ours.

Adaptation state

As mentioned in the *Chromatic transforms and the neural equiluminance constancy assumption* section, variations in MPOD, LPOD, and PPOD can alter the mean quantal catch levels of the cones. These mean changes affect both the numerators and denominators of the cone contrasts, and so cancel out, mimicking the effects of cone-specific adaptation. However, substantial changes in cone adaptation do alter visual processing and, using the same 6561 model observers, we have calculated these changes for our primaries for all three cone types (see the Appendix for details). Example cone fundamentals are shown in the top row of Figure 11. The fundamentals are not normalized in this figure to illustrate the vertical shifts that produce the major changes in cone adaptation level. The calculated adapting levels themselves, produced by multiplying the primary lights with the cone fundamental and integrating, then adding the results for the three primaries (Equations. A3 and A5), are shown in the bottom row of Figure 11. The adapting levels are in arbitrary units; here they are scaled relative to the standard observer, which is shown as a black dot in each panel. For MPOD and LPOD, increasing the density moves the cone fundamentals down, especially for the S-cone fundamental, thus reducing total quantal catch, whereas higher PPOD shifts the cone fundamentals up and thus increases the quantal catch for all three cone types. These changes in cone adaptation state are generally small, with only the effect of macular pigment on S-cones being appreciable (approximately one log unit) over our chosen ranges.

We derived linear models to describe the relationship between the adapting states, relative to the standard observer, and the four factors:

$$\frac{L_{adapt,i}}{L_{adapt,SS}} = 0.709 - 0.214 \ MPOD$$
$$- 0.113 \ LPOD + 1.153 \ PPOD$$
$$+ 0.005 \ \text{L-}\lambda_{max} \ \text{shift} \left(R^2 = 0.98\right) \qquad (6)$$
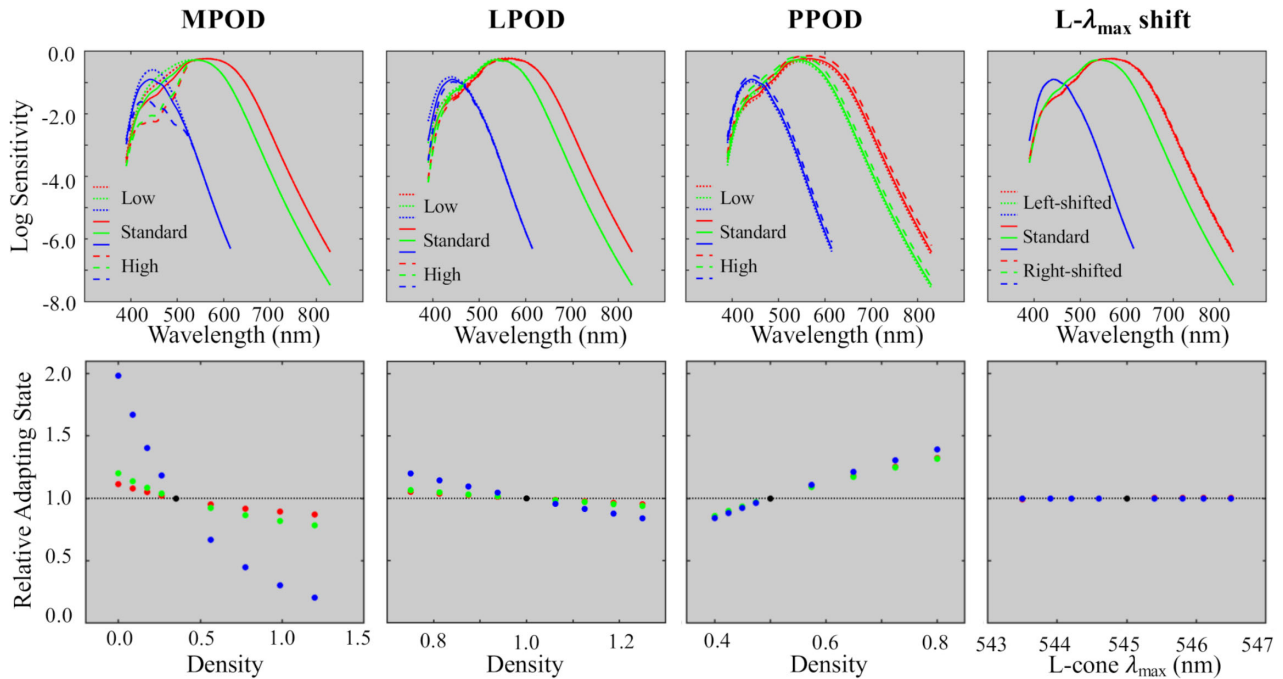
Figure 11. Effects of changes in the four factors on the cone fundamentals and the relative adapting states. The top row shows the corresponding cone fundamentals of the maximum and the minimum density (or left-shifted and right-shifted λ_{max}) of the factors. The curves are not normalized to show the vertical shifts. The bottom row shows the adapting states of the cones relative to the standard (represented by the black dot). The red, green, and blue dots represent the adapting states of L-, M-, and S-cones; all three cone types are plotted at all positions but may be hidden behind other symbols.

$$\frac{M_{adapt,i}}{M_{adapt,SS}} = 0.851 - 0.359 \, MPOD - 0.149 LPOD$$

$$+ 1.126 \, PPOD \, \left(\text{R}^2 = 0.96\right) \qquad (7)$$

$$\frac{S_{adapt,i}}{S_{adapt,SS}} = 1.797 - 1.539 \, MPOD - 0.422 LPOD$$

$$+ 1.369 \, PPOD \, \left(\text{R}^2 = 0.89\right) \qquad (8)$$

Conclusions

We used the neural equiluminance constancy assumption to calculate the effects due to MPOD, LPOD, PPOD, and changes in L-cone λ_{max}, while being agnostic about whether individuals *also* differ in L/M cone weights (k_1/k_2, Equation 1). Individual differences in equiluminance based upon HFP have often been interpreted as being due to differences in the L:M cone number in the retina (Brainard et al., 2000; Gunther & Dobkins, 2002; Kremers et al., 2000; Rushton & Baker, 1964), which in principle could alter k_1/k_2

(Equation 1), although those cone weights might also reflect postretinal factors. Clearly, extreme variation in the relative numbers of L- and M-cones must affect the equiluminance setting; in the limit imposed by dichromacy, $\alpha_{HFP} = 90°$ for a deuteranope and 180° for a protanope, and less extreme changes could also be reflected in k_1/k_2. In color normals, L:M cone number ratios measured by adaptive optics imaging or retinal densitometry agree well with electroretinogram (ERG) measurements (Brainard et al., 2000), and ERG and HFP estimates also provide similar ratios of L:M response (Gunther, Neitz, & Neitz, 2006; Kremers et al., 2000). Rushton and Baker (1964) reported a high correlation between the L/M ratios estimated by HFP and retinal densitometry (in observers who have extreme L- or M-cone sensitivities). They also found a more modest, but statistically significant, correlation between HFP and Rayleigh matches. This latter correlation is consistent with the neural equiluminance constancy assumption, since changes in cone fundamentals produce changes in Rayleigh matches. Rushton and Baker (1964) discounted the HFP/Rayleigh match correlation, focusing instead on the larger one between HFP and densitometry, but both effects were found.

Our main result is that almost all of the variation in our measured HFP settings (20 of 22 observers) could be attributed to individual differences in macular pigment density and photopigment optical density, with
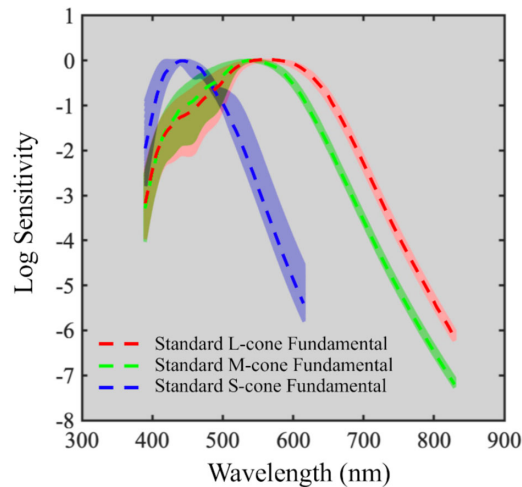
Figure 12. Effects of changes in the four factors on the cone fundamentals for the 6561 observers we modeled. The red, green, and blue dashed curves represent the standard L-, M-, and S-cone fundamentals. The shaded red, green, and blue areas around the dashed curves show the individual variations in cone fundamentals of the model observers, using the ranges summarized in Table 1.

smaller contributions from lens optical density and L-cone serine/alanine polymorphisms. These individual differences affect the settings through each observer's cone fundamentals, as illustrated in Figure 12. Varying the four physiological factors, over the ranges we selected, changed the α_{HFP} from 91.5° to 134°, corresponding to measured cone contrast ratios of -38.19 to -1.04, without varying the relative amount of L- and M-cone input into the luminance mechanism (k_1/k_2, Equation 1). One implication of our results is that without independently estimating the levels of MPOD, PPOD, LPOD, and cone polymorphisms for individual subjects, it will be difficult to determine the relationship between relative cone numerosity and HFP settings. Similar but more limited conclusions were made by Bieber et al. (1998) based upon modeling and by Carroll, McMahon, Neitz, and Neitz (2000) based upon ERG evidence. In contrast, very recently, Lee et al. (2020) argued that L/M ratio could be estimated from equiluminance settings independently from LPOD and MPOD, when equiluminance is determined using three primary (matched to a fourth, standard) lights (Webster, personal communication, June 2021). Our results apply to the more common case where there are only three primary lights, and specifically to the case where L- and M-cones are modulated while attempting to keep the S-cones unmodulated. Under these circumstances, our results indicate that changes in cone weights cannot be distinguished from variations in MPOD, LPOD, PPOD, and L-cone λ_{max}.

Clearly, individual differences in cone fundamentals can have large effects on heterochromatic flicker photometry, and presumably on other psychophysical tasks as well. That fact raises the possibility that the neural equiluminance constancy assumption may well be more than just a computational convenience as used here: individuals might in fact have the same k_1/k_2 ratio, despite there being variation in L:M cone numerosity. That constancy would likely result from a long-term, high-level adaptation (see Webster (2015) for a review) to the relative number of L- and M-cones in an individual's eye. Testing that idea would require estimating the low-level factors that determine the cone fundamentals.

Keywords: flicker photometry, HFP, individual differences, equiluminance, cone fundamentals

Acknowledgments

Footnote

[1]An angle of 122.8° would minimize photometric luminance (CIE 1924) modulation.

References

Asano, Y., Fairchild, M. D., & Blonde, L. (2016). Individual colorimetric observer model. *PLoS One, 11*(2), e0145671, doi:10.1371/journal.pone.0145671.

Beatty, S., Murray, I. J., Henson, D. B., Carden, D., Koh, H., & Boulton, M. E. (2001). Macular pigment and risk for age-related macular degeneration in subjects from a Northern European population. *Investigative Ophthalmology & Visual Science, 42*(2), 439–446.

Berendschot, T. T., van de Kraats, J., & van Norren, D. (1996). Foveal cone mosaic and visual pigment density in dichromats. *The Journal of Physiology, 492*(1), 307–314, doi:10.1113/jphysiol.1996.sp021310.

Bieber, M. L., Kraft, J. M., & Werner, J. S. (1998). Effects of known variations in photopigments on

L/M cone ratios estimated from luminous efficiency functions. *Vision Research, 38*(13), 1961–1966, doi:10.1016/s0042-6989(97)00302-7.

Bone, R. A., Landrum, J. T., & Cains, A. (1992). Optical density spectra of the macular pigment in vivo and in vitro. *Vision Research, 32*(1), 105–110, doi:10.1016/0042-6989(92)90118-3.

Bone, R. A., & Sparrock, J. M. B. (1971). Comparison of macular pigment densities in human eyes. *Vision Research, 11*(10), 1057–1064, doi:10.1016/0042-6989(71)90112-x.

Brainard, D. H., Roorda, A., Yamauchi, Y., Calderone, J. B., Mehta, A., Neitz, M., Neitz, J., Williams, D. R., & Jacobs, G. H. (2000). Functional consequences of the relative numbers of L and M cones. *Journal of the Optical Society of America A, 17*(3), 607–614, doi:10.1364/JOSAA.17.000607.

Brainard, D. H., & Stockman, A. (2010). Colorimetry. In M. Bass, C. DeCusatis, J. Enoch, V. Lakshminarayanan, G. Li, C. Macdonald, V. Mahajan, & E. van Stryland (Eds.), *The Optical Society of America Handbook of Optics (3rd ed., Volume III: Vision and Vision Optics)* (pp. 10.1–10.56). New York, NY: McGraw Hill.

Carroll, J., McMahon, C., Neitz, M., & Neitz, J. (2000). Flicker-photometric electroretinogram estimates of L:M cone photoreceptor ratio in men with photopigment spectra derived from genetics. *Journal of the Optical Society of America A, 17*(3), 499–509, doi:10.1364/josaa.17.000499.

Carroll, J., Neitz, J., & Neitz, M. (2002). Estimates of L:M cone ratio from ERG flicker photometry and genetics. *Journal of Vision, 2*(8), 531–542, doi:10.1167/2.8.1.

Eskew, R. T., Jr., McLellan, J. S., & Giulianini, F. (1999). Chromatic detection and discrimination. In K. R. Gegenfurtner, & L. T. Sharpe (Eds.), *Color vision: From genes to perception* (pp. 345–368). Cambridge, UK: Cambridge University Press.

Estévez, O., & Spekreijse, H. (1982). The "silent substitution" method in visual research. *Vision Research, 22*(6), 681–691.

Gibson, K. S., & Tyndall, E. P. T. (1923). Visibility of radiant energy. *Scientific Papers of the Bureau of Standards, 19*, 131–191, doi:10.6028/nbsscipaper.154.

Golz, J., & MacLeod, D. I. (2003). Colorimetry for CRT displays. *Journal of the Optical Society of America A, 20*(5), 769–781, doi:10.1364/josaa.20.000769.

Gunther, K. L., & Dobkins, K. R. (2002). Individual differences in chromatic (red/green) contrast sensitivity are constrained by the relative number of L- versus M-cones in the eye. *Vision Research, 42*(11), 1367–1378, doi:10.1016/S0042-6989(02)00043-3.

Gunther, K. L., Neitz, M., & Neitz, J. (2006). L:M cone contribution to heterochromatic flicker photometry. *Investigative Ophthalmology & Visual Science, 47*(13):1.

He, J., Taveras Cruz, Y., & Eskew, R. T., Jr. (2020). Methods for determining equiluminance in terms of L/M cone ratios. *Journal of Vision, 20*(4):22, doi:10.1167/jov.20.4.22.

Kremers, J., Scholl, H. P., Knau, H., Berendschot, T. T., Usui, T., & Sharpe, L. T. (2000). L/M cone ratios in human trichromats assessed by psychophysics, electroretinography, and retinal densitometry. *Journal of the Optical Society of America A, 17*(3), 517–526, doi:10.1364/JOSAA.17.000517.

Lee, K. R., Richardson, A. J., Walowit, E., Crognale, M. A., & Webster, M. A. (2020). Predicting color matches from luminance matches. *Journal of the Optical Society of America A, 37*(4), A35–A43, doi:10.1364/JOSAA.381256.

Merbs, S. L., & Nathans, J. (1992). Absorption spectra of human cone pigments. *Nature, 356*(6368), 433–435, doi:10.1038/356433a0.

Neitz, J., & Jacobs, G. H. (1990). Polymorphism in normal human color vision and its mechanism. *Vision Research, 30*(4), 621–636, doi:10.1016/0042-6989(90)90073-t.

Norren, D. V., & Vos, J. J. (1974). Spectral transmission of the human ocular media. *Vision Research, 14*(11), 1237–1244, doi:10.1016/0042-6989(74)90222-3.

Pease, P. L., Adams, A. J., & Nuccio, E. (1987). Optical density of human macular pigment. *Vision Research, 27*(5), 705–710, doi:10.1016/0042-6989(87)90067-8.

Pokorny, J., Smith, V. C., & Lutze, M. (1987). Aging of the human lens. *Applied Optics, 26*(8), 1437–1440, doi:10.1364/AO.26.001437.

Ripamonti, C., Woo, W. L., Crowther, E., & Stockman, A. (2009). The S-cone contribution to luminance depends on the M- and L-cone adaptation levels: Silent surrounds? *Journal of Vision, 9*(3), 1–16, doi:10.1167/9.3.10.

Rushton, W. A. H., & Baker, H. D. (1964). Red/green sensitivity in normal vision. *Vision Research, 4*(1-2), 75–85, doi:10.1016/0042-6989(64)90034-3.

Sharpe, L. T., Stockman, A., Jagla, W., & Jägle, H. (2005). A luminous efficiency function, V*(λ), for daylight adaptation. *Journal of Vision, 5*(11), 948–968, doi:10.1167/5.11.3.

Sharpe, L. T., Stockman, A., Jagla, W., & Jägle, H. (2011). A luminous efficiency function, VD65*(λ), for daylight adaptation: a correction.

Color Research and Application, 36(1), 42–46, doi:10.1002/col.20602.

Sharpe, L. T., Stockman, A., Jägle, H., Knau, H., Klausen, G., Reitner, A., & Nathans, J. (1998). Red, green, and red-green hybrid pigments in the human retina: Correlations between deduced protein sequences and psychophysically measured spectral sensitivities. *Journal of Neuroscience, 18*(23), 10053–10069, doi:10.1523/JNEUROSCI.18-23-10053.1998.

Stockman, A., Langendörfer, M., & Sharpe, L. T. (2007). Human short-wavelength-sensitive cone light adaptation. *Journal of Vision, 7*(3):4, 1–17, doi:10.1167/7.3.4.

Stockman, A., MacLeod, D. I., & DePriest, D. D. (1991). The temporal properties of the human short-wave photoreceptors and their associated pathways. *Vision Research, 31*(2), 189–208, doi:10.1016/0042-6989(91)90111-h.

Stockman, A., & Sharpe, L. T. (2000). The spectral sensitivities of the middle- and long-wavelength-sensitive cones derived from measurements in observers of known genotype. *Vision Research, 40*(13), 1711–1737, doi:10.1016/s0042-6989(00)00021-3.

Stockman, A., Sharpe, L. T., & Fach, C. (1999). The spectral sensitivity of the human short-wavelength sensitive cones derived from thresholds and color matches. *Vision Research, 39*(17), 2901–2927. doi:10.1016/S0042-6989(98)00225-9

Webster, M. A. (2015). Visual adaptation. *Annual Review of Vision Science, 1*, 547–567, doi:10.1146/annurev-vision-082114-035509.

Webster, M. A., & MacLeod, D. I. (1988). Factors underlying individual differences in the color matches of normal observers. *Journal of the Optical Society of America A, 5*(10), 1722–1735, doi:10.1364/josaa.5.001722.

Appendix

Monitor primaries

Our goal in this project was to model the individual differences in HFP settings that were measured using a SONY CRT monitor and our red (x = 0.607, y = 0.344), green (x = 0.287, y = 0.601), and blue (x = 0.152, y = 0.081) primaries. Figure A1 plots the measured spectra of the primaries at their maximum radiance levels; these energy spectra were converted to quantal units and used in the computations below (as R(λ), G(λ), and B(λ)). The quantitative details of the analysis
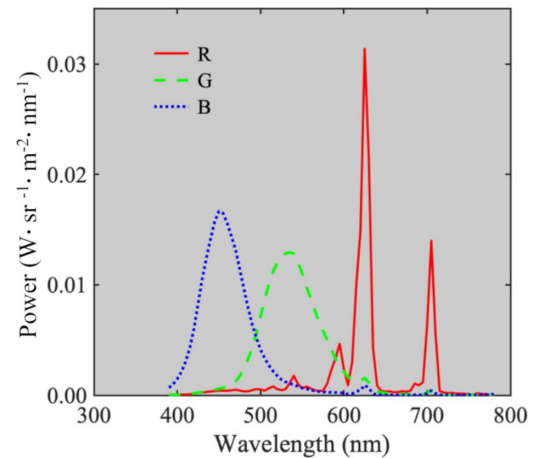

Figure A1. The spectral power distribution of our SONY GDM-F520 CRT monitor. Red, green, and blue curves represent the red, green, and blue channels, respectively.

would be at least somewhat different when applied to a different set of primary lights, since the elements of the matrix for transforming primaries to cone contrasts (Equation A1, below) are determined by the choice of primaries as well as the cone fundamentals that have been the focus of this study. However, the main points of this article are very likely to apply to other sets of primary lights. Preliminary calculations based upon an LCD stimulator designed for vision research (the VIEWPixx/3D display, from VPixx Technologies Inc., Saint-Bruno, QC Canada) produce qualitatively similar findings, in that a wide range of equiluminance angles, and thus M:L cone contrast ratios, can be achieved by the same realistic variations in cone fundamentals as shown here for the CRT, without consideration of other possible factors such as cone numbers.

Chromatic transformation between primaries and cone contrasts

We assume that the relationship between the monitor stimuli and the cone contrasts is linear (which is effectively assuming that the monitor was bright enough that the nonzero black level could be ignored). Thus there is a 3 × 3 matrix transformation between a vector of primary light contrasts **p** (each of which varies between −1 and +1), and the vector of three cone contrasts **c** (Eskew et al., 1999). For observer *i*,

$$\mathbf{c}_i = \mathbf{N}_i \cdot \mathbf{p} \tag{A1}$$

$$\begin{bmatrix} (\Delta L/L)_i \\ (\Delta M/M)_i \\ (\Delta S/S)_i \end{bmatrix} = \mathbf{N}_i \cdot \begin{bmatrix} r \\ g \\ b \end{bmatrix} \tag{A2}$$

The matrix N_i maps the RGB stimuli to cone contrasts. It consists of the product of two 3×3 matrices, $\mathbf{A^{-1}}$ and $\mathbf{D}$, corresponding to the denominator and numerator of the cone contrasts:

$$\mathbf{A_i} = \begin{bmatrix} RL_i + GL_i + BL_i & 0 & 0 \\ 0 & RM_i + GM_i + BM_i & 0 \\ 0 & 0 & RS_i + GS_i + BS_i \end{bmatrix} \quad \text{(A3)}$$

$$\mathbf{D_i} = \begin{bmatrix} RL_i & GL_i & BL_i \\ RM_i & GM_i & BM_i \\ RS_i & GS_i & BS_i \end{bmatrix} \quad \text{(A4)}$$

The nine distinct elements of these matrices are the inner products of the spectra of the red, green, and blue primary channels of the display (in quantal units) and the three cone fundamentals (in quantal sensitivity units), and thus represent the cone excitation of one cone type produced by one of the primary lights at the midpoint of their radiances (i.e., at the adapting condition); for example, for the red primary and the L-cones,

$$RL_i = \frac{1}{2} \int_{390}^{780} R(\lambda) L_i(\lambda) \, d\lambda \quad \text{(A5)}$$

The diagonal elements of $\mathbf{A}$ represent the adaptation states of the three cones; these are plotted in the bottom row of Figure 11. When $\mathbf{A}$ is inverted it produces the three denominators of the cone contrasts. Thus, the transformation in Equation (A2) is accomplished by having

$$\mathbf{N_i} = \mathbf{A_i^{-1}} \mathbf{D_i} \quad \text{(A6)}$$

Note that if the three diagonal elements of $\mathbf{A}$ are set to 1.0, the same computation creates cone excitations (in arbitrary units) instead of cone contrasts. If instead these three diagonal elements were set to L, M, and S threshold values, the computation would be made in threshold units. Neither of these changes would have altered any of the conclusions of this study.

For the standard observer, $L_i(\lambda)$ is the quantal Stockman-Sharpe L-cone fundamental $(L_{SS}(\lambda))$, and similarly for the M- and S-cone fundamentals $(M_{SS}(\lambda)$ and $S_{SS}(\lambda))$. For the other model observers, L-cone functions (as well as the corresponding M- and S-cone functions) were recalculated, starting from the Stockman-Sharpe absorbance curves and adding in the effects of L-cone λ_{max} shift, photopigment peak density, macular pigment density, and lens optical density (Brainard & Stockman, 2010). The changes in

the physiological factors, therefore, produce changes in cone fundamentals. Each set of fundamentals renders a different N_i for converting between RGB vectors and LMS cone contrast vectors.

To calculate a vector of RGB primary stimuli p for the ith observer, we have from Equation (A1)

$$\mathbf{N_i^{-1}} \cdot \mathbf{c_i} = \mathbf{p} \quad \text{(A7)}$$

RGB stimuli for the standard observer

Let the elements of the inverse matrix (Equation A7) for the standard observer be

$$\mathbf{N_{SS}^{-1}} = \begin{bmatrix} SS_{11} & SS_{12} & SS_{13} \\ SS_{21} & SS_{22} & SS_{23} \\ SS_{31} & SS_{32} & SS_{33} \end{bmatrix}$$

in which each SS value is a constant. For the stimuli in the experiment, S-cone modulation was kept at zero for the standard observer, so that in Equation A7,

$$\begin{bmatrix} SS_{11} & SS_{12} & SS_{13} \\ SS_{21} & SS_{22} & SS_{23} \\ SS_{31} & SS_{32} & SS_{33} \end{bmatrix} \cdot \begin{bmatrix} (\Delta L/L)_{SS} \\ (\Delta M/M)_{SS} \\ 0 \end{bmatrix} = \begin{bmatrix} r \\ g \\ b \end{bmatrix}$$

Solving for the blue coordinate after eliminating $(\Delta L/L)_{SS}$ and $(\Delta M/M)_{SS}$,

$$b = \frac{r(SS_{21}SS_{32} - SS_{22}SS_{31}) + g(SS_{12}SS_{31} - SS_{11}SS_{32})}{SS_{12}SS_{21} - SS_{11}SS_{22}}, \quad \text{(A8)}$$

a plane in RGB space. This is the yellow plane shown in Figure A2, below (and represented illustratively in Figure 2); the experiment was designed such that all
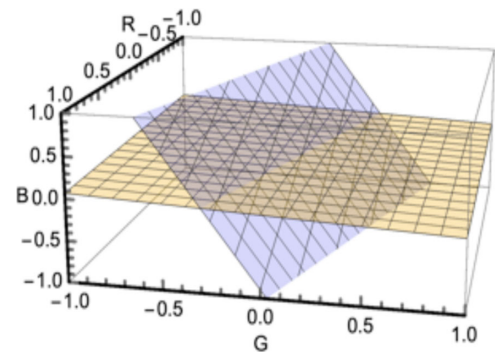

Figure A2. Two planes in the RGB primary space. In the nearly flat yellow plane, the S-cones of the standard observer are unmodulated; this plane is represented schematically in Figure 2. The blue plane represents stimuli for which $(\Delta M/M) = -2(\Delta L/L)$ for one of the other model observers (observer Z).

the HFP stimuli lay in that plane. This plane is nearly, but not exactly, orthogonal to the B axis, indicating that only small modulations in the blue primary are required to cancel the green primary's effect on the S-cones and leave them unmodulated. According to the model, $k_1/k_2 = 2$ (Equation 2), so the standard observer selects the RGB in that plane that produces a $-2:1$ ratio of M:L contrasts when calculated via the standard cone fundamentals. That computation is described next, for a nonstandard observer (but it is the same calculation that is used for the standard observer).

RGB stimuli for a nonstandard observer

The model sets $k_1/k_2 = 2$ (Equation 2) for *all* observers (the neural equiluminance constancy assumption), and thus for each observer the ratio of M-to-L contrasts at equiluminance is -2 in terms of their own cone fundamentals. For a nonstandard observer Z (with cone fundamentals shown in Figure 2),

$$\mathbf{N}_Z^{-1} \cdot \begin{bmatrix} (\Delta L/L)_Z \\ -2(\Delta L/L)_Z \\ (\Delta S/S)_Z \end{bmatrix} = \begin{bmatrix} r \\ g \\ b \end{bmatrix}_Z \quad (A9)$$

with nine constants

$$\mathbf{N}_Z^{-1} = \begin{bmatrix} Z_{11} & Z_{12} & Z_{13} \\ Z_{21} & Z_{22} & Z_{23} \\ Z_{31} & Z_{32} & Z_{33} \end{bmatrix}$$

determined by use of their nonstandard cone fundamentals. Solving for the b coordinate in Equation A9 after eliminating $(\Delta L/L)_Z$ and $(\Delta S/S)_Z$

$$b = \frac{r[Z_{21}Z_{33} + 2(Z_{23}Z_{32} - Z_{22}Z_{33}) - Z_{23}Z_{31}] + g[Z_{13}Z_{31} + 2(Z_{12}Z_{33} - Z_{13}Z_{32}) - Z_{11}Z_{33}]}{Z_{13}Z_{21} + 2(Z_{12}Z_{23} - Z_{13}Z_{22}) - Z_{11}Z_{23}},$$

$$(A10)$$

another plane in RGB. An example for extreme observer Z is shown as the blue plane in Figure A2. This

is the model observer with lowest values of MPOD, PPOD, LPOD, and a leftward L-λ_{max} shift, whose cone fundamentals are plotted in Figure 2 and whose results are plotted in blue in Figure 9.

Intersection of the two stimulus planes

Figure A2 shows, in the primary stimulus space, the intersection of the $\Delta S/S = 0$ plane for the standard observer, and the plane defined by $(\Delta M/M)/(\Delta L/L) = -2$ for a nonstandard observer.

The line of intersection of these two planes represents all the RGB stimuli that satisfy both constraints. This line may be found by solving Equation A8 for *r*, and substituting that into Equation A10. The point at which that line meets the gamut limits (where $max(|r|, |g|, |b|) = 1$) represents the peak of the HFP setting at maximum contrast for observer *Z*: that is the stimulus $\mathbf{p}_Z$ from those used in the experiment that produces an individual M:L contrast ratio of -2 (of course this would also be true had the blue plane been calculated using the standard cone fundamentals, using $\mathbf{N}^{-1}_{SS}$ in Equation A9). Calculating $\mathbf{N}_Z \cdot \mathbf{p}_Z$ (from Equation A9) provides the actual S-cone contrast—using individual cone fundamentals—for the nonstandard observer (as reported in the *S-cone modulation* section of Results and Discussion). That RGB is then transformed into Stockman-Sharpe cone contrasts

$$\mathbf{c}_i = \mathbf{N}_{SS} \cdot \mathbf{p}_Z$$

as was done for each of the HFP settings in the analysis of the actual experimental data. The vector of Stockman-Sharpe cone contrasts c_i must have $(\Delta S/S)_{SS} = 0$, but it will not, in general, have a $-2:1$ M:L ratio; the analysis of the obtained ratios (and their corresponding angles in the Stockman-Sharpe LM plane) forms the major result of the study.